People’s Democratic Republic of Algeria
Ministry of Higher Education and Scientific Research

University of Saida – Dr. Moulay Tahar

Faculty of Mathematics, Computing and Telecommunications

Department of Telecommunications

Master Thesis

Submitted in partial fulfilment of the requirements for the Master’s Degree in Telecommunications Systems

---

Impact of Antenna Position on the Performance of Microwave Brain Imaging for Medical Diagnosis

---

Presented by:

AMEUR Fatima Zohra
BRAHIMI Nihad

Supervised by:

Prof. MANSOURI Boualam

Defended on 15 June 2026 before the jury composed of:

Name	Grade	Role
Mr. BOURAS Bouhafs	MCA	President
Prof. MANSOURI Boualam	Professor	Supervisor
Prof. BOUHMIDI Rachid	Professor	Examiner

Academic Year: 2025/2026

Dedication

We dedicate this work to our parents, whose love, patience, and sacrifices have supported every step of our academic journey. Their encouragement and trust have been a permanent source of strength. This achievement is dedicated to them with deep respect and gratitude.

Acknowledgements

First, we thank Allah for granting us the strength and patience to complete this work. We express our sincere gratitude to our supervisor, Prof. MANSOURI Boualam, for his scientific guidance, advice, and continuous support. We also thank the jury members, Mr. BOURAS Bouhafs and Prof. BOUHMIDI Rachid, for their evaluation and constructive remarks. Our thanks are extended to the Department of Telecommunications and to the Faculty of Mathematics, Computing and Telecommunications at the University of Saida – Dr. Moulay Tahar.

Contents

List of Figures

List of Tables

List of Abbreviations

AVA	Antipodal Vivaldi Antenna
BAVA	Balanced Antipodal Vivaldi Antenna
CAD	Computer-Aided Design
CST	Computer Simulation Technology
CT	Computed Tomography
FDTD	Finite-Difference Time-Domain
GHz	Gigahertz
MRI	Magnetic Resonance Imaging
SAR	Specific Absorption Rate
TSA	Tapered Slot Antenna
UWB	Ultra-Wideband
VSWR	Voltage Standing Wave Ratio

General Introduction

Medical microwave brain imaging is an emerging diagnostic technique that uses low-power electromagnetic waves to detect abnormalities inside the human brain, particularly stroke, haemorrhage, and tumours. Compared with computed tomography and magnetic resonance imaging, microwave imaging has the advantages of being non-ionizing, potentially portable, relatively low cost, and compatible with rapid point-of-care assessment. Its physical principle is based on the fact that healthy and abnormal tissues exhibit different dielectric properties, which modify the amplitude, phase, and time delay of the backscattered microwave signal.

The antenna is a central element in such a system because it launches the incident wave into the head and collects the scattered field containing diagnostic information. Among many candidate antennas, the antipodal Vivaldi antenna is attractive because it offers ultra-wideband behaviour, directional radiation, compact planar geometry, and good time-domain fidelity. However, the antenna does not operate in free space during brain imaging. It is placed close to a lossy, heterogeneous, multilayered biological structure. Therefore, the antenna position relative to the head has a major effect on impedance matching, coupling efficiency, penetration, clutter, reverberation, and specific absorption rate.

This thesis studies the impact of antenna position on the performance of microwave brain imaging for medical diagnosis. The main objective is to determine how the antenna-to-head distance affects the electromagnetic behaviour of the antenna and the quality of the received signal. The work focuses on three distances, $D = 1$ cm, $D = 2$ cm, and $D = 4.5$ cm, and also studies the effect of side corrugations on the time-domain reflected waveform.

This dissertation is organized into three chapters. Chapter 1 presents the fundamentals of biomedical microwave imaging, including propagation, scattering, dielectric properties, and exposure safety. Chapter 2 introduces the Vivaldi antenna and discusses its geometry, operating principle, reflection coefficient, and relevance to microwave imaging. Chapter 3 provides the final full-wave simulation analysis, reorders the results

Chapter 1

Biomedical Brain Imaging

1.1 Introduction

Biomedical imaging has evolved from purely anatomical visualization toward multimodal systems capable of providing structural, functional, and electromagnetic information about the human body. Modern medical systems increasingly use concepts from telecommunications and electromagnetics because radiofrequency and microwave waves can penetrate biological media, interact with tissue properties, and support noninvasive sensing.

Microwave brain imaging is investigated as a complementary diagnostic modality for neurological abnormalities. Its interest comes from three main features: microwave radiation is non-ionizing, the hardware can be compact and portable, and the measurement is sensitive to tissue dielectric contrast. This makes microwave imaging attractive for applications where rapid screening or continuous monitoring is required.

1.2 Microwave Frequency Fundamentals

1.2.1 Electromagnetic Spectrum

The electromagnetic spectrum includes radiation from low-frequency radio waves to high-frequency gamma rays. Microwaves occupy the region between radio-frequency waves and infrared radiation. They are generally associated with frequencies from approximately 300 MHz to 300 GHz. In biomedical imaging, only selected sub-bands are used because the operating frequency must balance penetration depth and spatial resolution.

The relationship between frequency and free-space wavelength is

$$\lambda_0 = \frac{c}{f}, \tag{1.1}$$

where λ_0 is the free-space wavelength, c is the speed of light, and f is the frequency. Lower frequencies have longer wavelengths and generally penetrate biological tissue more deeply, while higher frequencies provide better spatial resolution but suffer from stronger attenuation.

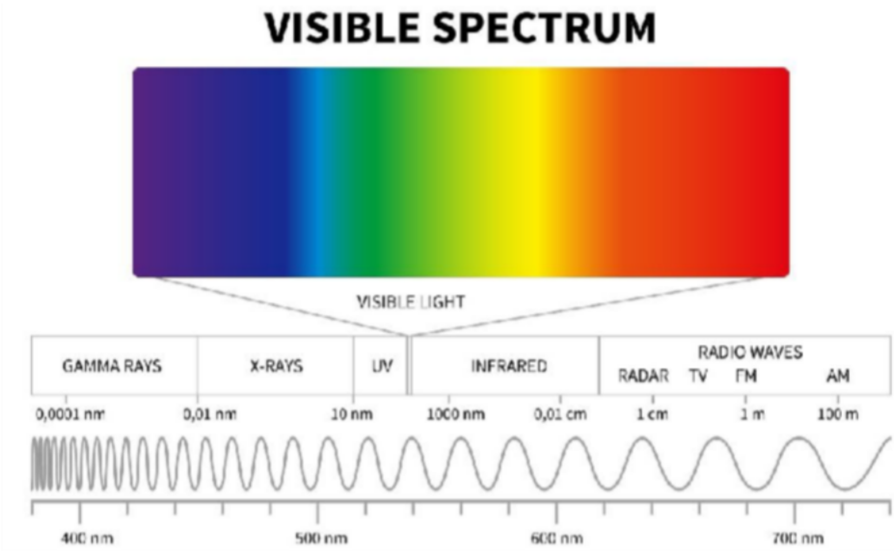

Figure 1.1: Electromagnetic spectrum including the microwave region.

1.2.2 Propagation in Biological Tissues

Biological tissues are lossy and heterogeneous dielectric media. When a microwave wave enters tissue, its amplitude decreases because part of the electromagnetic energy is absorbed and converted into heat. The electric field in a lossy medium may be expressed as

$$E(z) = E_0 e^{-\alpha z} e^{-j\beta z}, \tag{1.2}$$

where E_0 is the initial field amplitude, α is the attenuation constant, β is the phase constant, and z is the propagation distance.

At an interface between two tissues, part of the incident field is reflected. For normal incidence, the reflection coefficient can be approximated by

$$\Gamma = \frac{Z_2 - Z_1}{Z_2 + Z_1}, \tag{1.3}$$

where Z_1 and Z_2 are the intrinsic impedances of the two media. Large dielectric mismatch, such as the air-skull interface, increases reflection and can create strong clutter in microwave brain imaging.

1.2.3 Scattering and Signal Interaction

Scattering is the redirection of the electromagnetic wave caused by dielectric inhomogeneities. In biomedical microwave imaging, scattering is the main source of diagnostic information. A lesion, tumour, haemorrhage, or stroke region can produce a scattered signal because its electrical properties differ from those of surrounding healthy tissue.

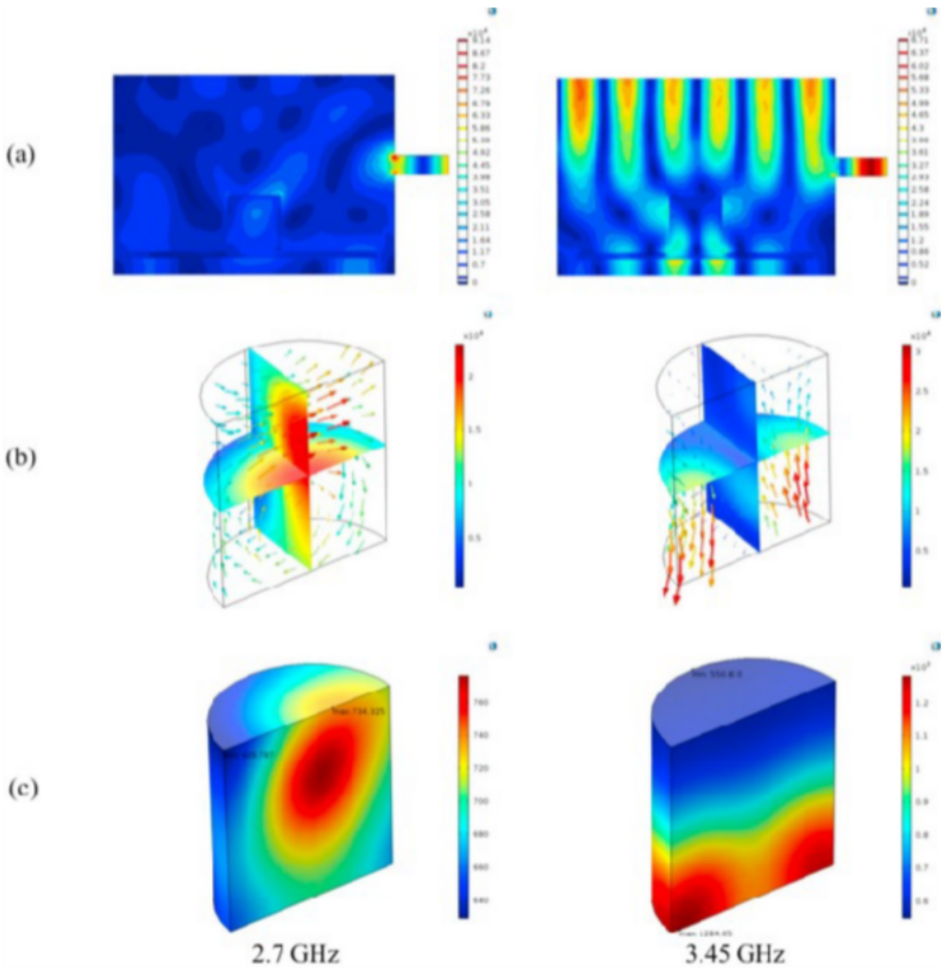

Figure 1.2: Simulation examples of microwave propagation and scattering in biological media.

The measured response can be decomposed as

$$S_{\text{meas}} = S_{\text{direct}} + S_{\text{boundary}} + S_{\text{sca}} + n, \tag{1.4}$$

where S_{direct} is the direct coupling component, S_{boundary} is the reflection from normal tissue boundaries, S_{sca} is the useful scattered contribution, and n represents noise. The objective of microwave imaging is to preserve and interpret S_{sca} while reducing clutter.

1.3 Microwave Interaction with Biological Tissues

1.3.1 Complex Permittivity

The dielectric response of a biological tissue is described by its complex permittivity:

$$\varepsilon^* = \varepsilon' - j\varepsilon'', \tag{1.5}$$

where ε' represents energy storage and ε'' represents energy loss. For conductive tissues, the loss term is related to conductivity by

$$\varepsilon^* = \varepsilon' - j\frac{\sigma}{\omega}, \tag{1.6}$$

where σ is the conductivity and $\omega = 2\pi f$ is the angular frequency.

The loss tangent is defined as

$$\tan\delta = \frac{\varepsilon''}{\varepsilon'}, \tag{1.7}$$

which indicates the ratio between dissipated and stored energy. High-water-content tissues such as blood and muscle usually present higher permittivity and conductivity than fatty tissues, leading to stronger attenuation and scattering.

1.3.2 Specific Absorption Rate

Safety in microwave exposure is evaluated by the specific absorption rate:

$$SAR = \frac{\sigma|E|^2}{2\rho}, \tag{1.8}$$

where ρ is the tissue mass density. SAR increases with conductivity and electric-field magnitude. Therefore, antenna position, input power, and field concentration must be controlled in biomedical systems.

The absorbed power can be related to incident and remaining power by

$$P_{\text{abs}} = P_{\text{in}} - P_{\text{out}}. \tag{1.9}$$

The corresponding temperature rise can be approximated by

$$\Delta T = \frac{P_{\text{abs}} t}{m c_p}, \tag{1.10}$$

where t is the exposure time, m is tissue mass, and c_p is the specific heat capacity.

1.4 Biomedical Microwave Imaging

1.4.1 Definition and Principle

Biomedical microwave imaging is a non-ionizing technique that reconstructs internal dielectric contrast from scattered microwave signals. The imaging problem can be described by a forward model:

$$\mathbf{d} = \mathcal{F}\{\chi(\mathbf{r})\} + \mathbf{n}, \tag{1.11}$$

where $\mathbf{d}$ is the measured data vector, $\mathcal{F}$ is the electromagnetic forward operator, $\chi(\mathbf{r})$ is the unknown contrast distribution, and $\mathbf{n}$ is measurement noise.

The purpose of reconstruction is to estimate $\chi(\mathbf{r})$ from $\mathbf{d}$. In delay-and-sum imaging, the image intensity at a point $\mathbf{r}$ can be conceptually written as

$$I(\mathbf{r}) = \sum_{m=1}^{M} w_m s_m \left(t_m(\mathbf{r})\right), \tag{1.12}$$

where M is the number of measurement channels, s_m is the received signal, $t_m(\mathbf{r})$ is the time delay associated with the point $\mathbf{r}$, and w_m is a weighting coefficient.

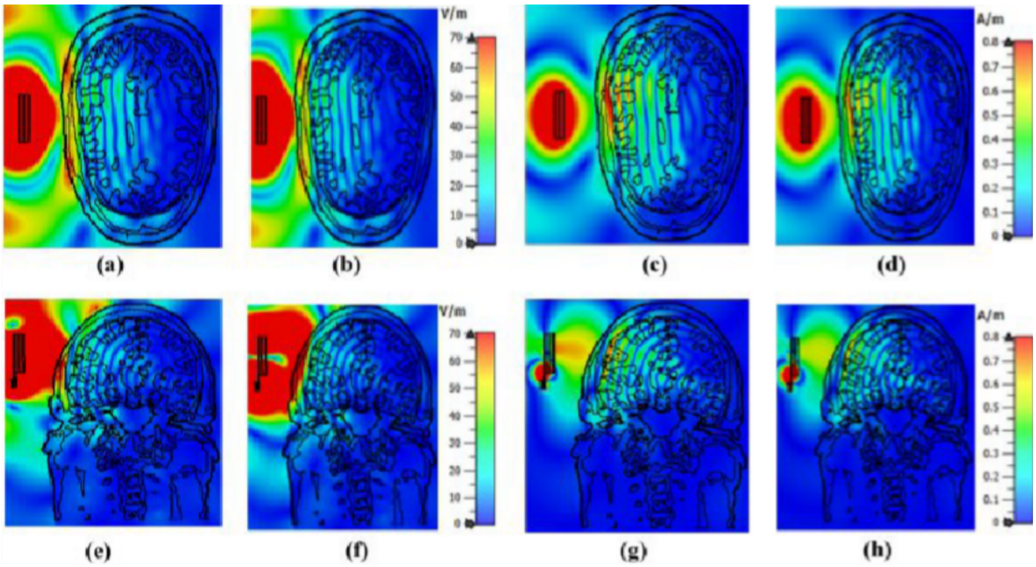

Figure 1.3: Forward problem in microwave brain imaging: multi-angle illumination and electromagnetic-field distortion inside a multilayered head structure.

1.4.2 Advantages and Limitations

Microwave imaging offers several advantages: non-ionizing operation, potential portability, sensitivity to dielectric contrast, and compatibility with low-cost hardware. Nevertheless, it also faces important limitations, including strong attenuation in lossy tissues, clutter caused by boundaries, antenna mutual coupling, calibration errors, and the ill-posed nature of the inverse problem.

A useful qualitative indicator of imaging quality is

$$Q_{\mathrm{img}} \propto \frac{C}{L+N}, \tag{1.13}$$

where C represents dielectric contrast, L represents propagation loss, and N represents noise and modelling uncertainty. This relation is not a strict physical law, but it summarizes the practical trade-off: imaging improves when contrast is high and losses are low.

1.5 Microwave Brain Imaging and Antenna Systems

Brain imaging is challenging because the human head is curved, multilayered, and strongly heterogeneous. The skull, cerebrospinal fluid, grey matter, white matter, and blood have different dielectric properties.

Therefore, the antenna system must provide wide bandwidth, directional radiation, stable matching, and safe exposure.

Antenna performance affects the received signal through the antenna transfer function:

$$V_{\text{rx}}(f) = H_a(f)V_{\text{tx}}(f), \tag{1.14}$$

where $H_a(f)$ is the frequency-dependent antenna response. Good imaging performance requires $H_a(f)$ to be sufficiently wideband and stable over the operating range.

The delivered power is linked to the input reflection coefficient by

$$P_{\text{del}} = P_{\text{in}}\left(1 - |\Gamma|^2\right). \tag{1.15}$$

A small $|\Gamma|$ improves the power transferred to the antenna and reduces measurement distortion.

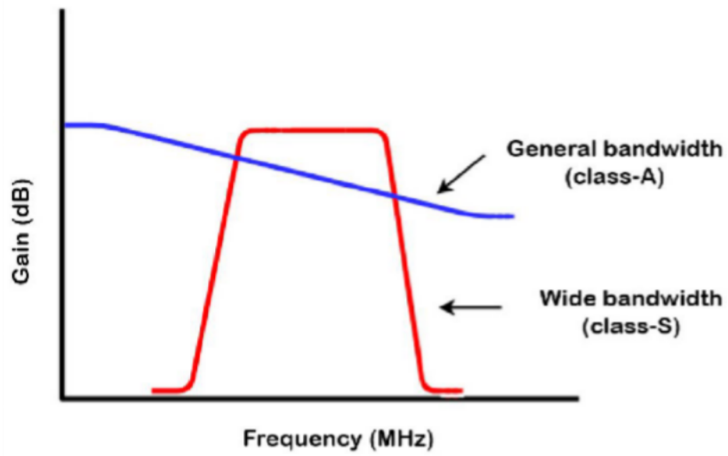

Figure 1.4: Illustration of the relationship between antenna gain and spectral bandwidth for narrowband and wideband systems.

1.6 Antennas Used in Microwave Imaging

Several antenna families have been used in microwave imaging, including monopole antennas, patch antennas, tapered slot antennas, and Vivaldi antennas. For brain imaging, the antenna must be compact, wideband, directive, and compatible with near-field operation. It must also have low ringing in the time domain, because excessive ringing can mask the weak scattered signal from internal tissue contrasts.

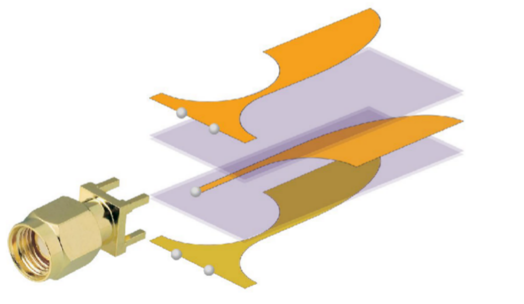

(a) Antipodal Vivaldi concept.

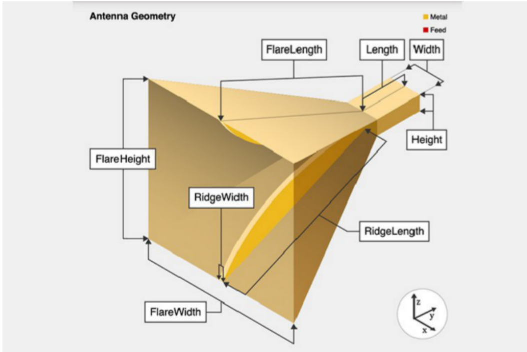

(b) Antenna geometry parameters.

Figure 1.5: Examples of antenna structures used in wideband microwave systems.

(a) Planar antenna array.

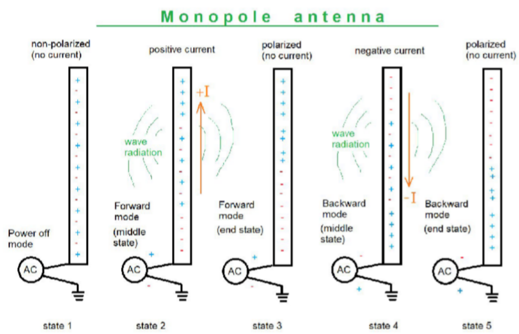

(b) Monopole antenna variants.

Figure 1.6: Examples of antenna concepts relevant to microwave imaging and sensing.

1.7 Conclusion

This chapter presented the theoretical background of biomedical microwave imaging. It explained microwave propagation, tissue interaction, dielectric contrast, scattering, SAR, and the central role of antennas. The chapter also clarified why antenna position is an important design parameter: it controls the balance between coupling strength, penetration, safety, and signal quality. These principles form the basis for the Vivaldi antenna design and the simulation study developed in the following chapters.

Chapter 2

Vivaldi Antenna Design and Characterization

2.1 Introduction

The Vivaldi antenna is a travelling-wave tapered-slot antenna widely used in ultra-wideband systems. It is well suited for microwave imaging because it can radiate over a broad frequency range while maintaining directional behaviour and good time-domain fidelity. This chapter introduces the operating principle, geometrical parameters, substrate choice, and reflection-coefficient characteristics of the Vivaldi antenna used in this thesis.

2.2 Overview of Vivaldi Antenna

A Vivaldi antenna uses an exponentially tapered slot to transform guided energy from the feed line into a radiated wave. The taper provides a gradual impedance transition, which is the main reason for the wideband behaviour. The antipodal Vivaldi antenna uses overlapping metal arms on opposite sides of the substrate, creating a smooth transition from a microstrip line to a balanced slot aperture.

The exponential taper can be written as

$$y(x) = c_1 e^{ax} + c_2, \tag{2.1}$$

where a controls the opening rate and c_1, c_2 are constants determined by the initial and final aperture points.

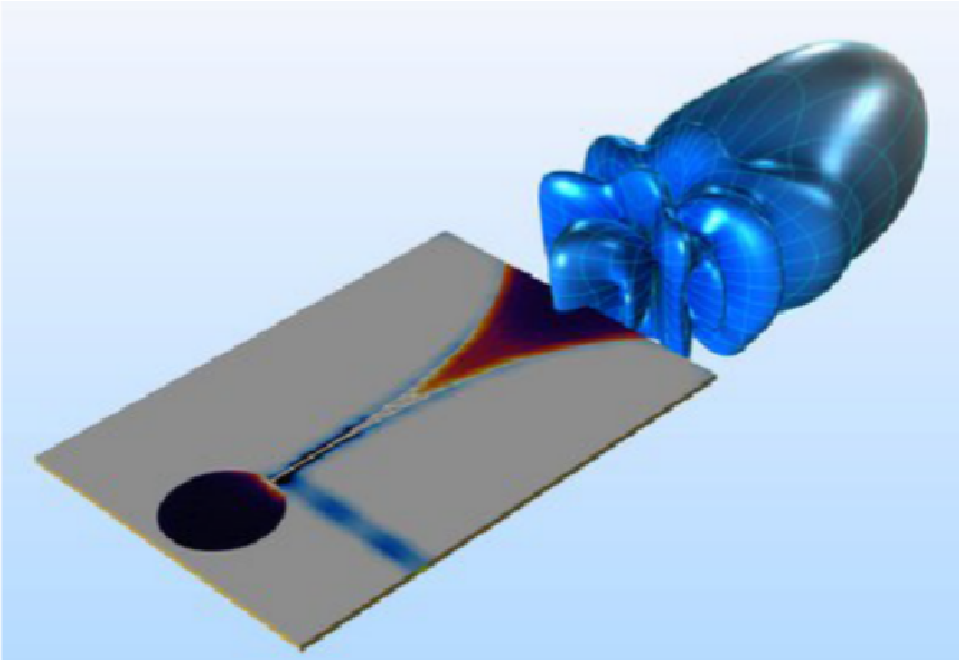

Figure 2.1: Three-dimensional numerical model of the ultra-wideband Vivaldi antenna used near a head model.

2.3 Operating Principle of the Vivaldi Antenna

The Vivaldi antenna operates as a broadband travelling-wave radiator. At lower frequencies, the active radiating region is located closer to the larger aperture, while at higher frequencies it moves toward narrower portions of the taper. This distributed radiation mechanism enables broadband impedance matching and stable directional radiation.

The far-field condition of a conventional antenna is usually approximated by

$$R_{\mathrm{ff}} \geq \frac{2D_a^2}{\lambda}, \tag{2.2}$$

where D_a is the largest antenna dimension and λ is the wavelength. In microwave brain imaging, however, the antenna operates mainly in the near-field region. Therefore, the antenna-to-head distance strongly affects the electromagnetic coupling and cannot be ignored.

2.4 Antenna Geometry and Structure

The antenna geometry includes the substrate, microstrip feed, antipodal tapered arms, and corrugated edges. The selected substrate is Rogers

RT6010 with relative permittivity

$$\varepsilon_r = 10.2, \tag{2.3}$$

and thickness

$$h = 0.64 \text{ mm}. \tag{2.4}$$

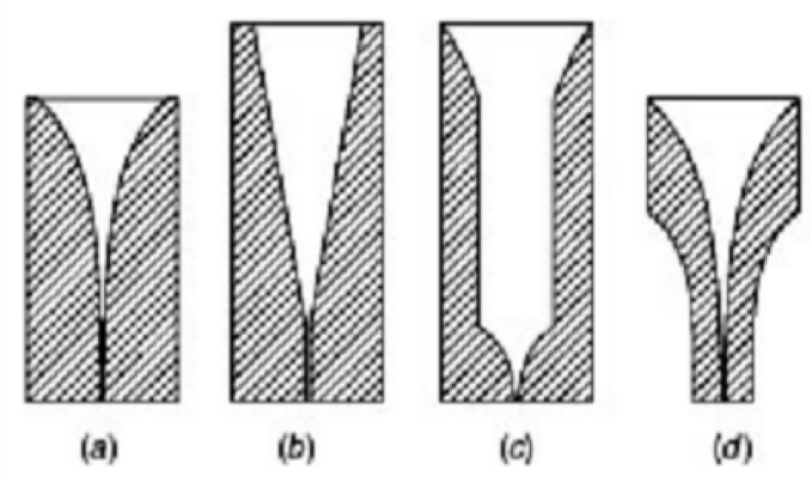

Figure 2.2: Illustrative Vivaldi antenna profiles showing the influence of taper and shape variations.

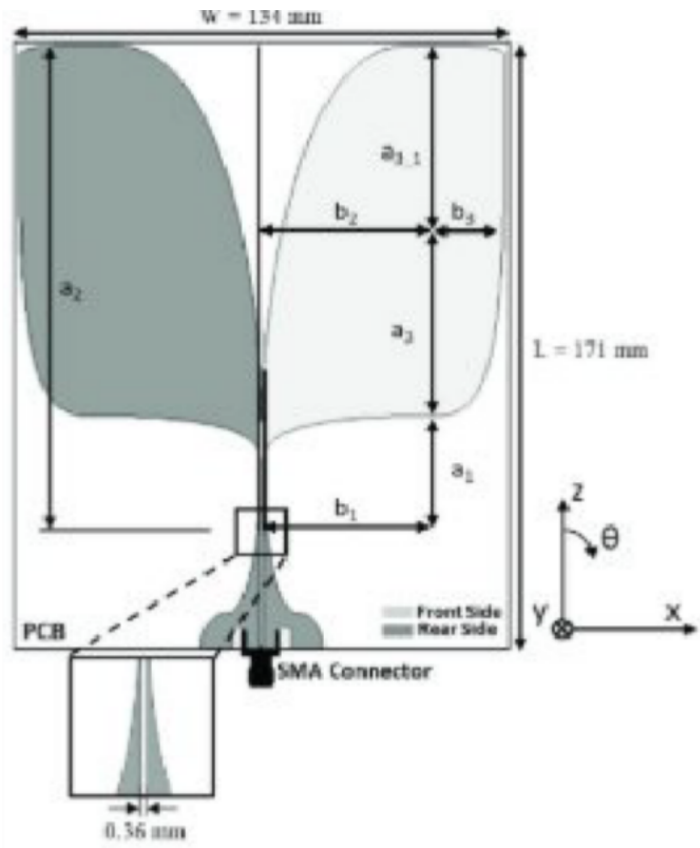

Figure 2.3: Main geometrical parameters of the designed antipodal Vivaldi antenna.

The antenna dimensions are selected to support compact integration around a head model while preserving wideband impedance matching. The use of corrugations modifies the current path and helps reduce unwanted reflection and ringing in the received signal.

2.5 Substrate Material Selection

Substrate selection is critical because permittivity, loss tangent, and thickness affect antenna size, bandwidth, radiation efficiency, and near-field coupling. A high-permittivity substrate reduces the antenna dimensions, which is useful for compact biomedical systems. However, higher permittivity can also increase stored energy and reduce bandwidth if the geometry is not properly optimized. The choice of Rogers RT6010 provides a compromise between compactness and wideband operation.

2.6 Reflection Coefficient S_{11}

The input reflection coefficient is defined as

$$\Gamma_{\text{in}} = \frac{Z_{\text{in}} - Z_0}{Z_{\text{in}} + Z_0}, \tag{2.5}$$

where Z_{in} is the antenna input impedance and $Z_0 = 50\ \Omega$ is the reference impedance. The corresponding reflection coefficient in decibels is

$$S_{11,\text{dB}} = 20 \log_{10} |\Gamma_{\text{in}}|. \tag{2.6}$$

A lower S_{11} value indicates better matching. For UWB microwave imaging, the antenna should maintain acceptable matching over a broad frequency range.

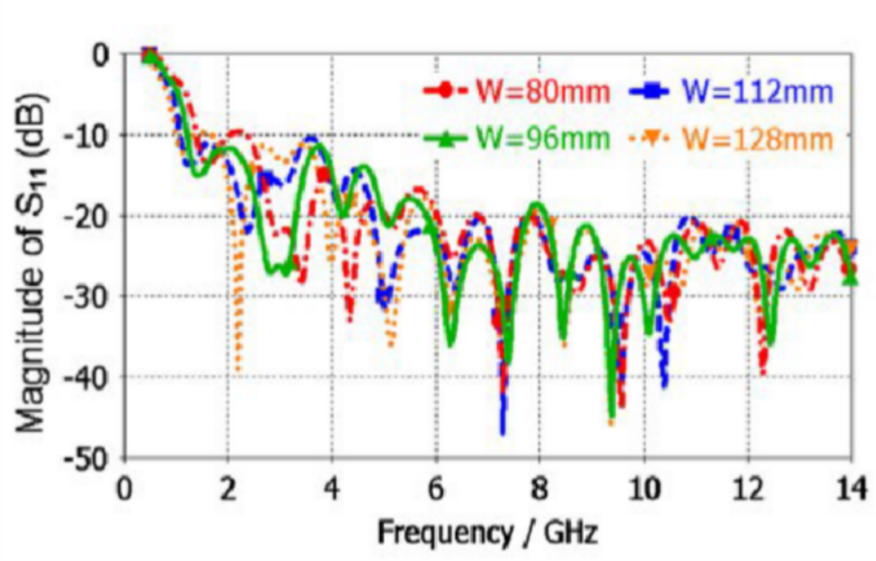

Figure 2.4: Effect of width variation on the reflection coefficient S_{11}.

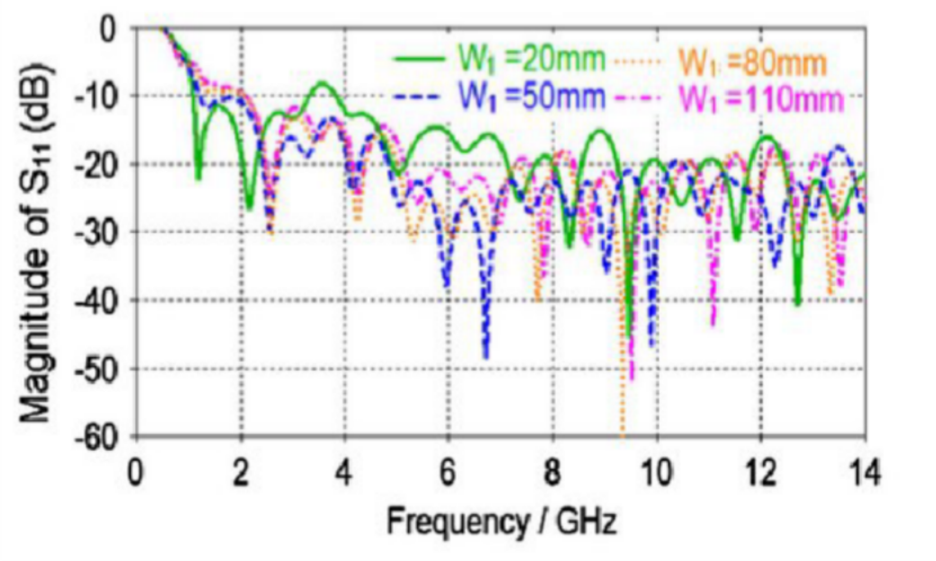

Figure 2.5: Effect of the parameter W_1 on the reflection coefficient S_{11}.

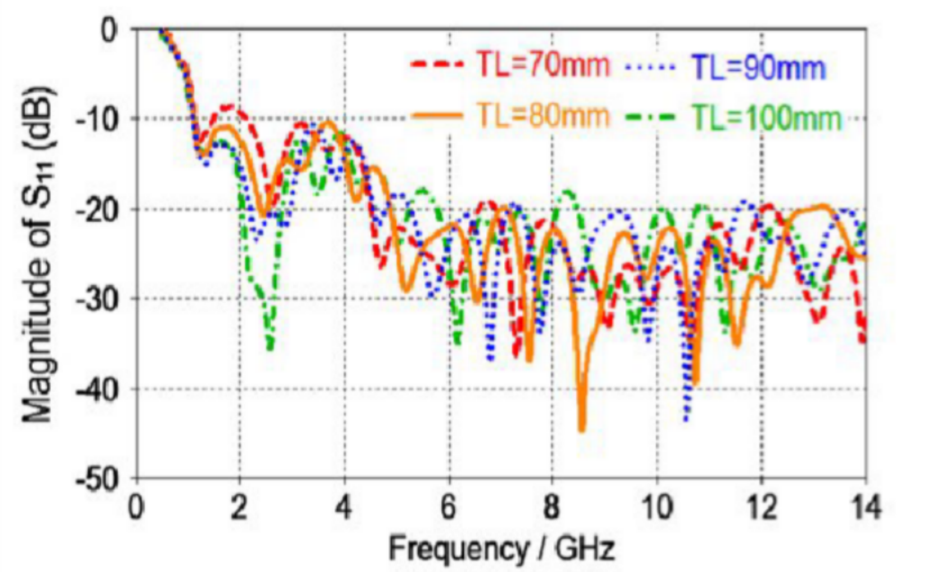

Figure 2.6: Effect of taper-length variation on the reflection coefficient S_{11}.

2.7 Applications in Microwave Imaging

Vivaldi antennas are suitable for microwave imaging because they offer wide bandwidth, directional radiation, and good time-domain pulse behaviour. In brain imaging, they can be integrated into a helmet-like array or used individually to analyse the effect of antenna placement. Their directional nature helps focus energy toward the head and reduces radiation in undesired directions.

2.8 Conclusion

This chapter presented the design and characterization principles of the antipodal Vivaldi antenna. The chapter described the tapered-slot operation, geometrical parameters, substrate choice, and reflection-coefficient behaviour. These elements are essential for understanding the simulation results in Chapter 3, where the antenna is placed at different distances from a head model and evaluated for microwave brain imaging.

Chapter 3

Simulation and Results

3.1 Introduction

This chapter presents the full-wave electromagnetic evaluation of the proposed compact antipodal Vivaldi antenna for microwave brain imaging. The chapter is reorganized to follow the scientific logic of the study: antenna and numerical configuration, electromagnetic evaluation criteria, antenna-to-head distance analysis, SAR interpretation, reflected-signal quality, corrugation optimization, comparative synthesis, and final discussion.

The main objective is to determine how the antenna position affects the imaging system performance. In microwave brain imaging, the antenna operates in the near field of a lossy and heterogeneous biological structure. Therefore, changing the antenna-to-head distance modifies the impedance matching, electromagnetic coupling, field penetration, safety constraint, and time-domain reflected signal.

Three distances are investigated:

$$D \in \{1 \text{ cm},\ 2 \text{ cm},\ 4.5 \text{ cm}\}. \tag{3.1}$$

These distances represent strong coupling, intermediate coupling, and weak coupling, respectively.

3.2 Investigated Antenna and Numerical Configuration

The investigated structure is a miniaturized antipodal Vivaldi antenna. It is implemented on Rogers RT6010 with

$$\varepsilon_r = 10.2, \qquad h = 0.64 \text{ mm}, \tag{3.2}$$

and has approximate dimensions

$$L \times W = 44.4 \text{ mm} \times 30.2 \text{ mm}. \tag{3.3}$$

The feed is designed for

$$Z_0 = 50 \ \Omega. \tag{3.4}$$

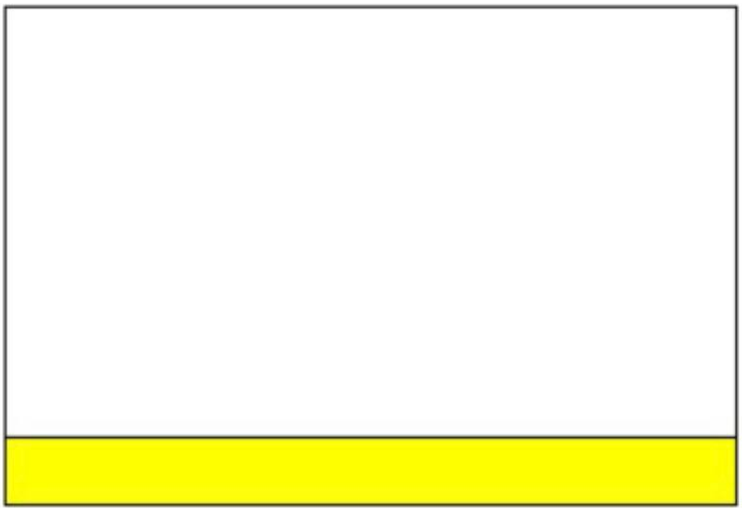

Figure 3.1: Initial structure of the proposed antenna showing the substrate and ground plane.

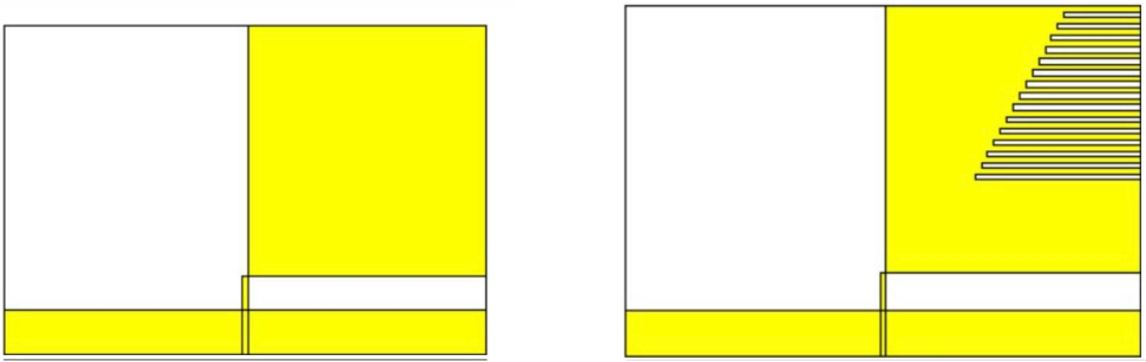

(a) Top layer before corrugation. **(b)** Top layer with corrugation.

Figure 3.2: Top-layer geometry of the proposed antipodal Vivaldi antenna before and after edge corrugation.

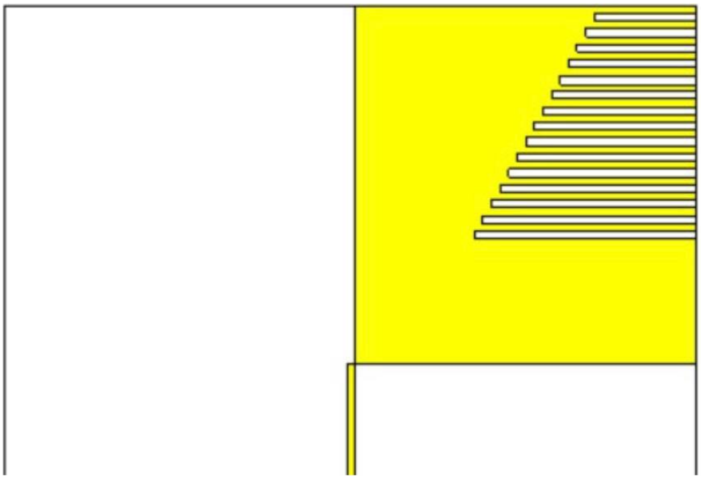

Figure 3.3: Bottom-layer geometry of the proposed antipodal Vivaldi antenna.

3.3 Electromagnetic Evaluation Criteria

The antenna performance is evaluated using the reflection coefficient, input impedance, surface current distribution, field intensity, SAR, and received time-domain signal. The input impedance is

$$Z_{\text{in}}(f) = R_{\text{in}}(f) + jX_{\text{in}}(f), \tag{3.5}$$

and the reflection coefficient in decibels is

$$S_{11,\text{dB}}(f) = 20 \log_{10} |\Gamma_{\text{in}}(f)|. \tag{3.6}$$

The received signal can be decomposed as

$$s_{\text{rx}}(t) = s_{\text{direct}}(t) + s_{\text{skin/skull}}(t) + s_{\text{reverb}}(t) + s_{\text{target}}(t) + n(t), \tag{3.7}$$

where $s_{\text{target}}(t)$ is the diagnostically useful backscattered component.

The 10-g averaged SAR is defined by

$$SAR = \frac{\sigma |E|^2}{2\rho}. \tag{3.8}$$

The maximum admissible input power is estimated as

$$P_{\text{max}} = P_{\text{sim}} \frac{SAR_{\text{lim}}}{SAR_{\text{sim}}}, \tag{3.9}$$

where $SAR_{\text{lim}} = 2$ W/kg.

3.4 Influence of Antenna-to-Head Distance

3.4.1 Surface Current Distribution

At $D = 1$ cm, the antenna is strongly loaded by the biological medium. The surface current is modified near the feed, taper, and corrugated edges. At $D = 2$ cm, the perturbation remains visible but becomes more balanced. At $D = 4.5$ cm, the antenna behaves closer to the free-space condition, but the useful coupling to the head is weaker.

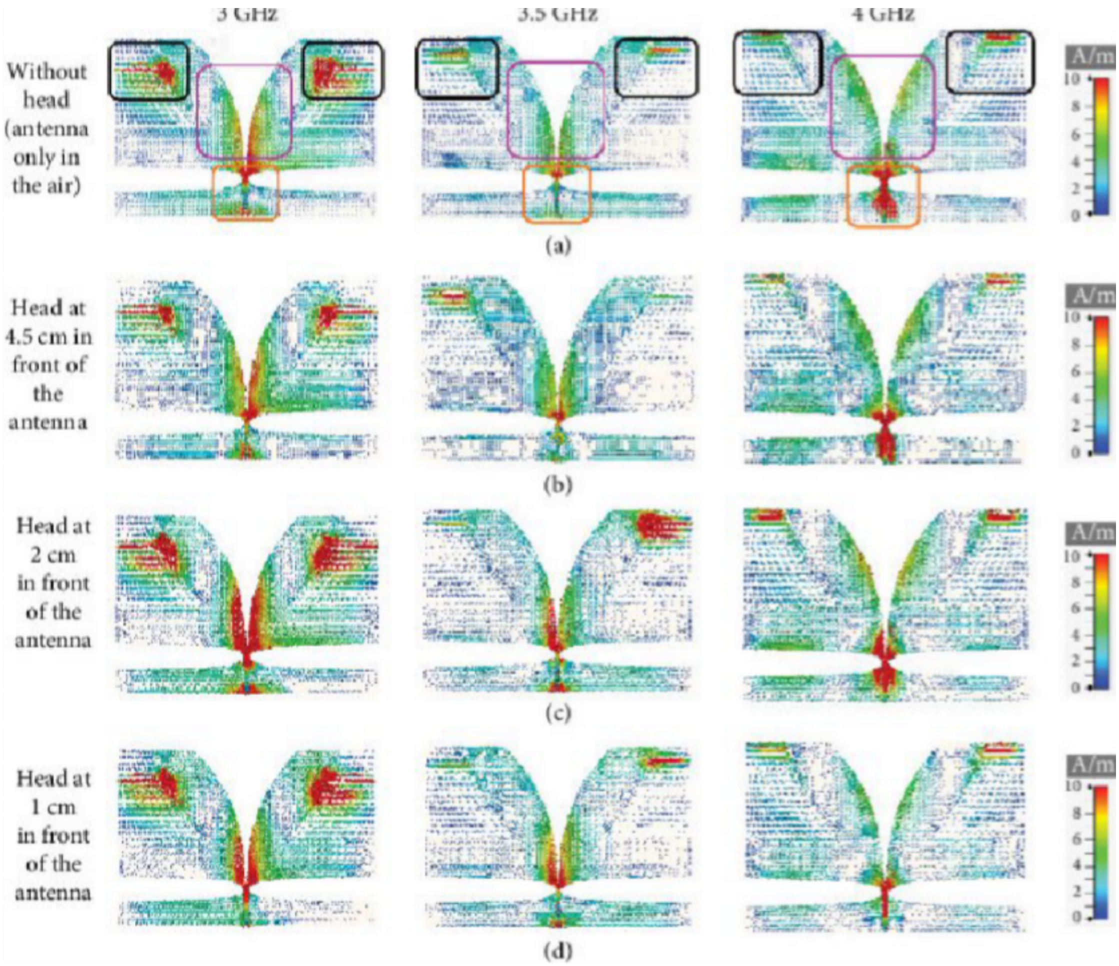

Figure 3.4: Effect of antenna-to-head distance on the surface current distribution at different operating frequencies.

3.4.2 Input Impedance and Matching Stability

The input impedance results confirm the loading effect. The real and imaginary parts are strongly perturbed for $D = 1$ cm, indicating high sensitivity to the head. The $D = 2$ cm case provides a more stable impedance response while preserving useful coupling. The $D = 4.5$ cm case is less perturbed but provides weaker interaction with the head.

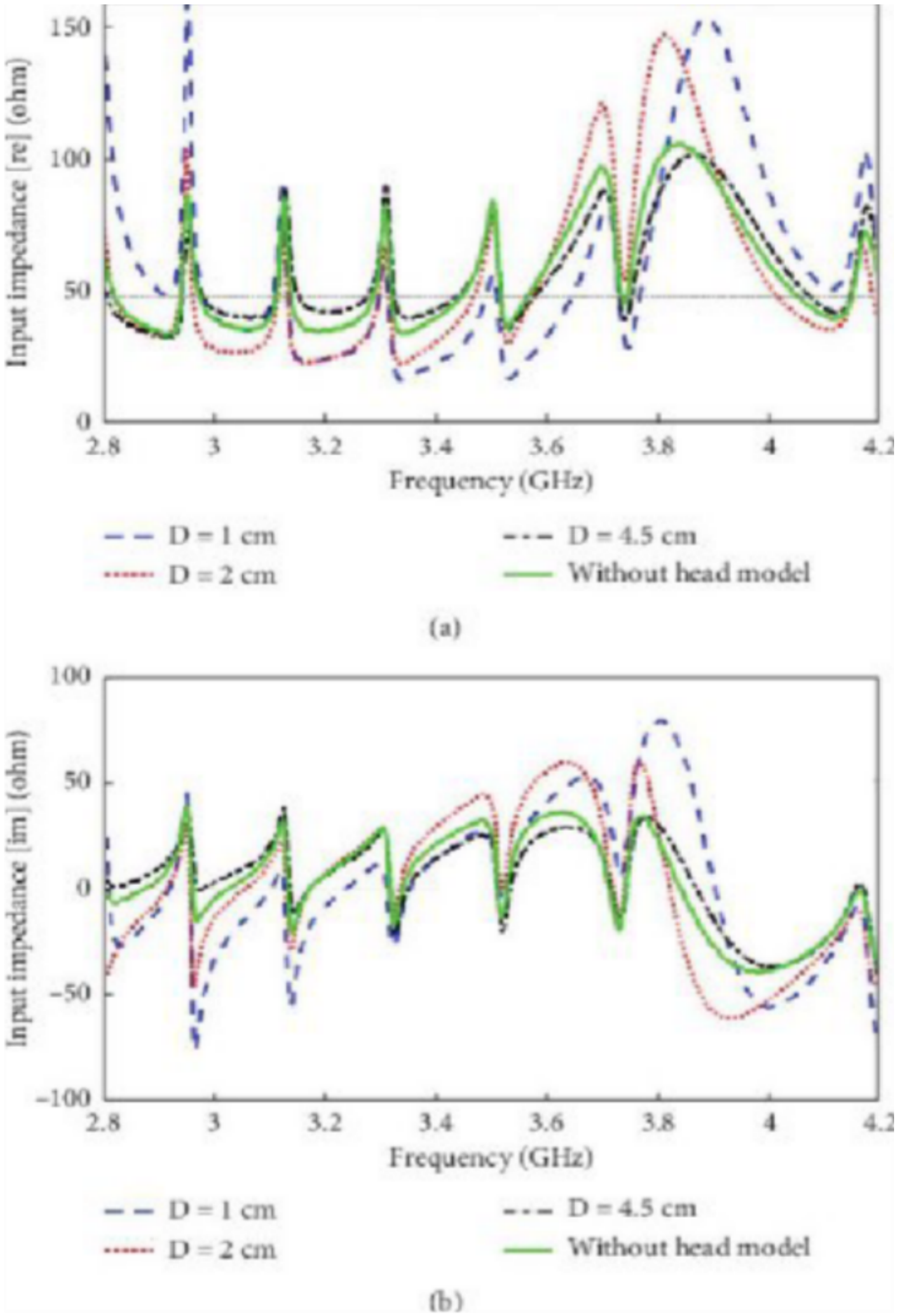

Figure 3.5: Real and imaginary parts of the input impedance for the investigated antenna-to-head distances.

3.4.3 Field Penetration

The field-depth results show that excessive proximity increases superficial field intensity but may not improve deep penetration. At $D = 1$ cm, the field is strong near the surface but decays rapidly. At $D = 2$ cm, the field distribution is more balanced. At $D = 4.5$ cm, the field reaching the head is reduced by spreading loss.

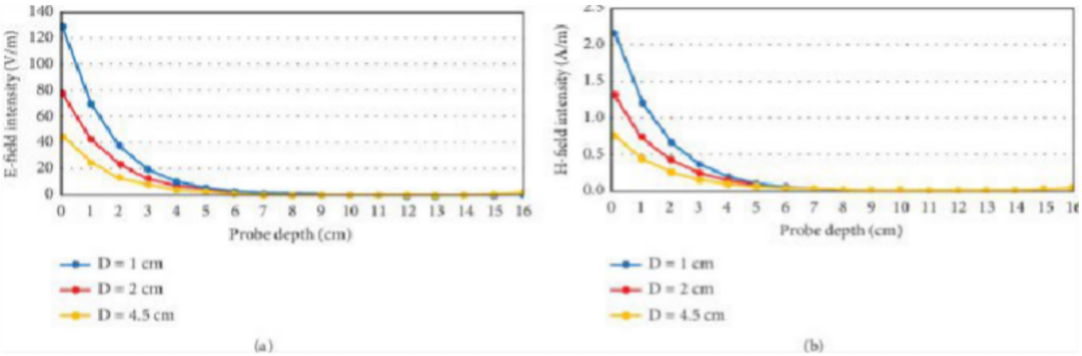

Figure 3.6: Electric-field and magnetic-field intensity versus probe depth for the investigated antenna-to-head distances.

3.4.4 SAR and Safety Constraint

Using Eq. (3.9), the maximum input power is approximately 0.13 W for $D = 1$ cm and 0.28 W for $D = 2$ cm. Therefore, increasing the distance from 1 cm to 2 cm improves the safety margin while preserving useful electromagnetic coupling.

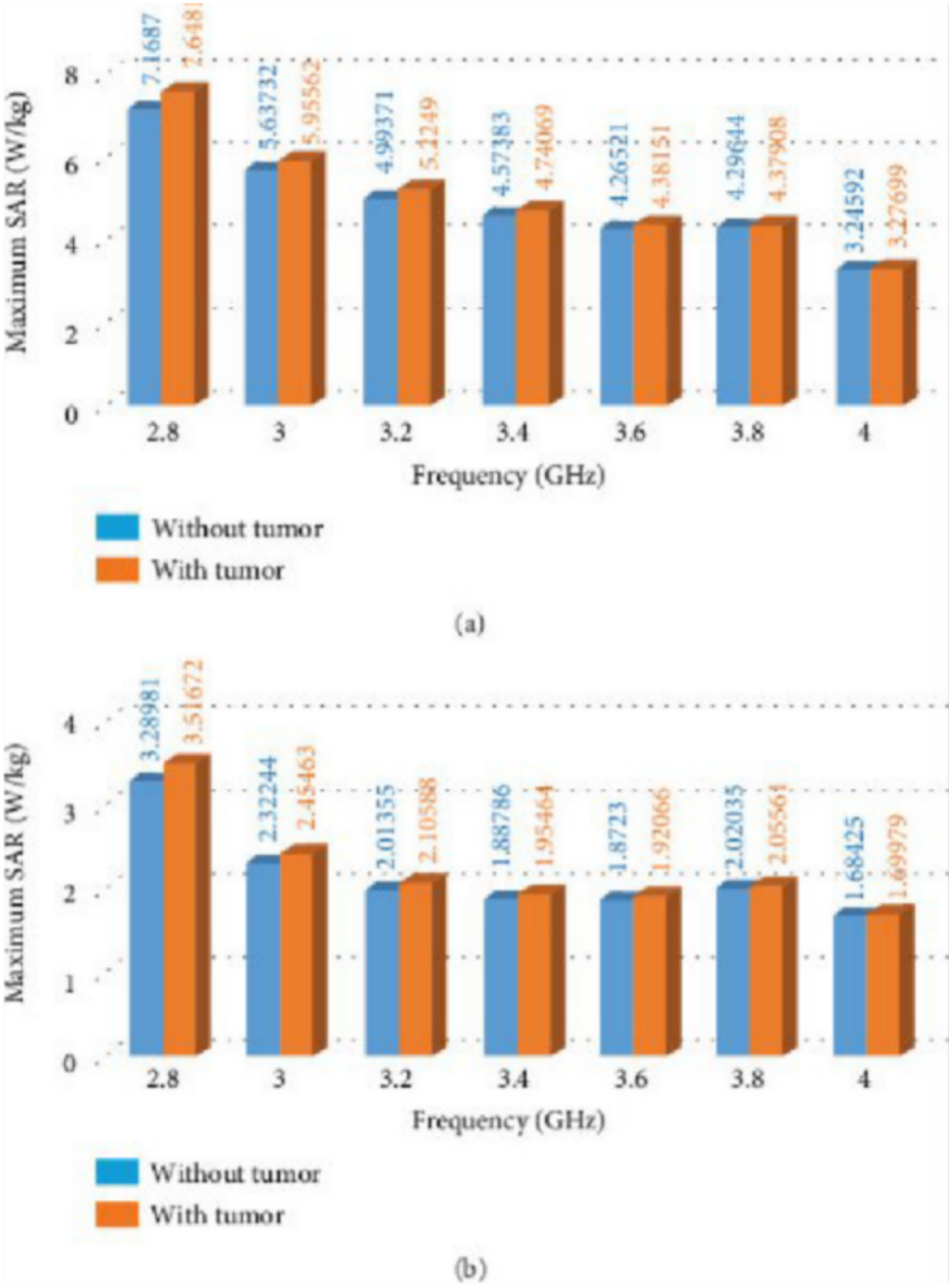

Figure 3.7: Maximum 10-g averaged SAR for $D = 1$ cm and $D = 2$ cm.

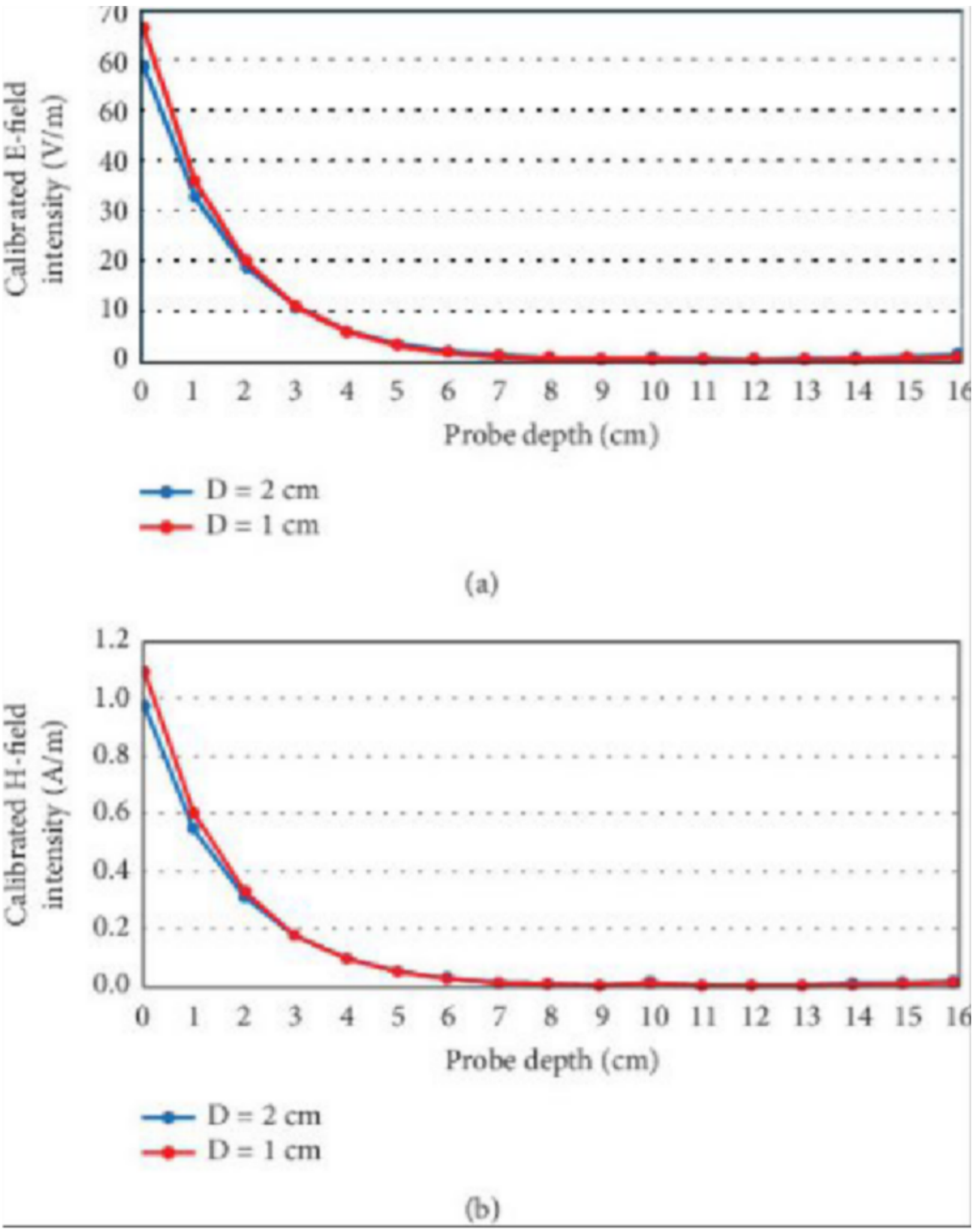

Figure 3.8: Calibrated electric- and magnetic-field intensities for $D = 1$ cm and $D = 2$ cm.

3.4.5 Time-Domain Reflected Signal

At $D = 1$ cm, the reflected waveform contains stronger early-time components and more visible reverberation. These effects are mainly caused by intense near-field coupling and reflections at the air-head interface. At $D = 2$ cm, the waveform becomes cleaner and reverberation decreases. At $D = 4.5$ cm, the useful signal becomes weaker because the antenna is farther from the head.

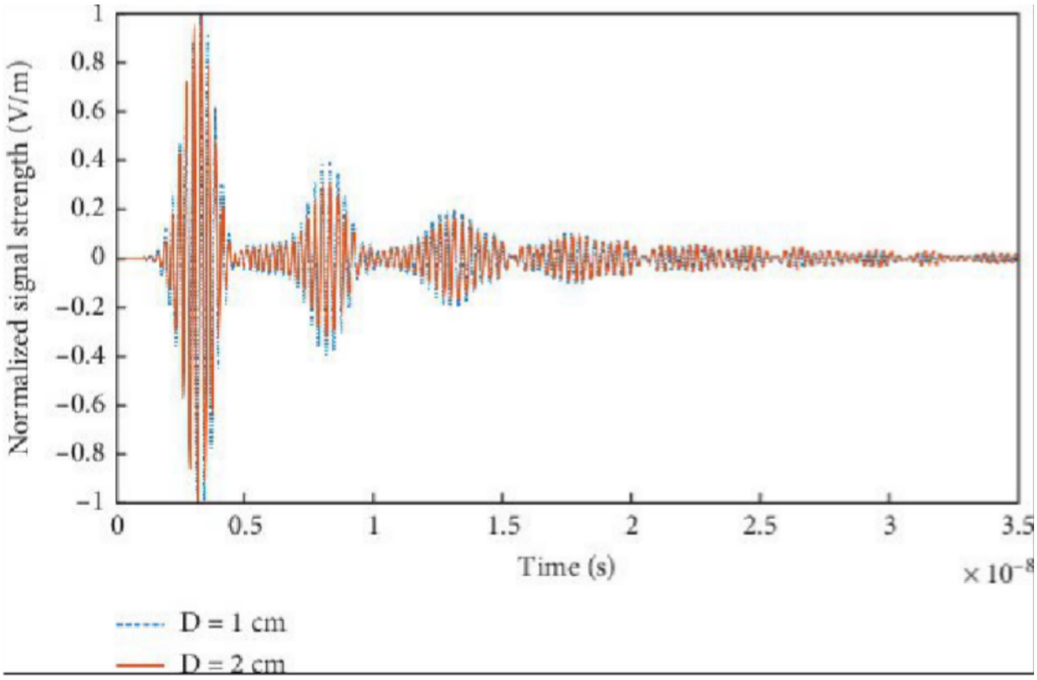

Figure 3.9: Reflected signal received by the antenna for different antenna-to-head distances.

3.5 Corrugation Optimization

The side corrugation profile is studied through the geometrical parameters a and d. These parameters modify the current path along the edges and affect internal reflections. The best time-domain behaviour is obtained for

$$a = 0.5 \text{ mm}, \qquad d = 0.5 \text{ mm}. \tag{3.10}$$

This configuration reduces late-time reverberation while preserving wide-band matching.

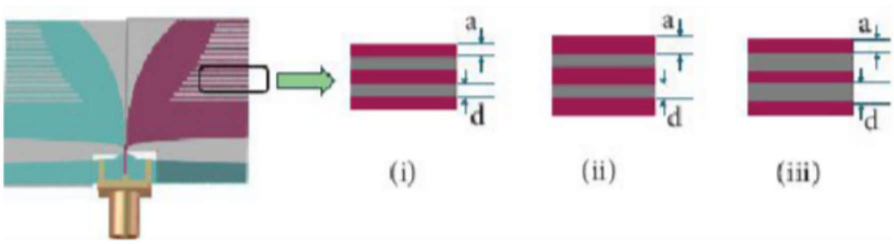

Figure 3.10: Corrugation profiles investigated for the antipodal Vivaldi antenna.

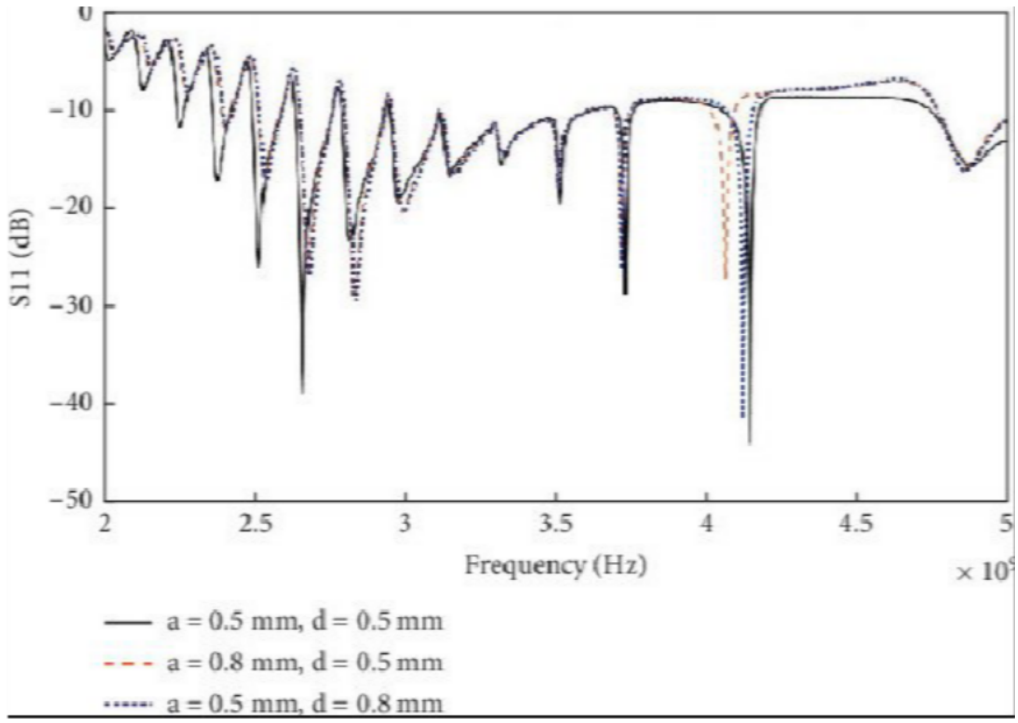

Figure 3.11: Effect of corrugation variations on the reflection coefficient S_{11}.

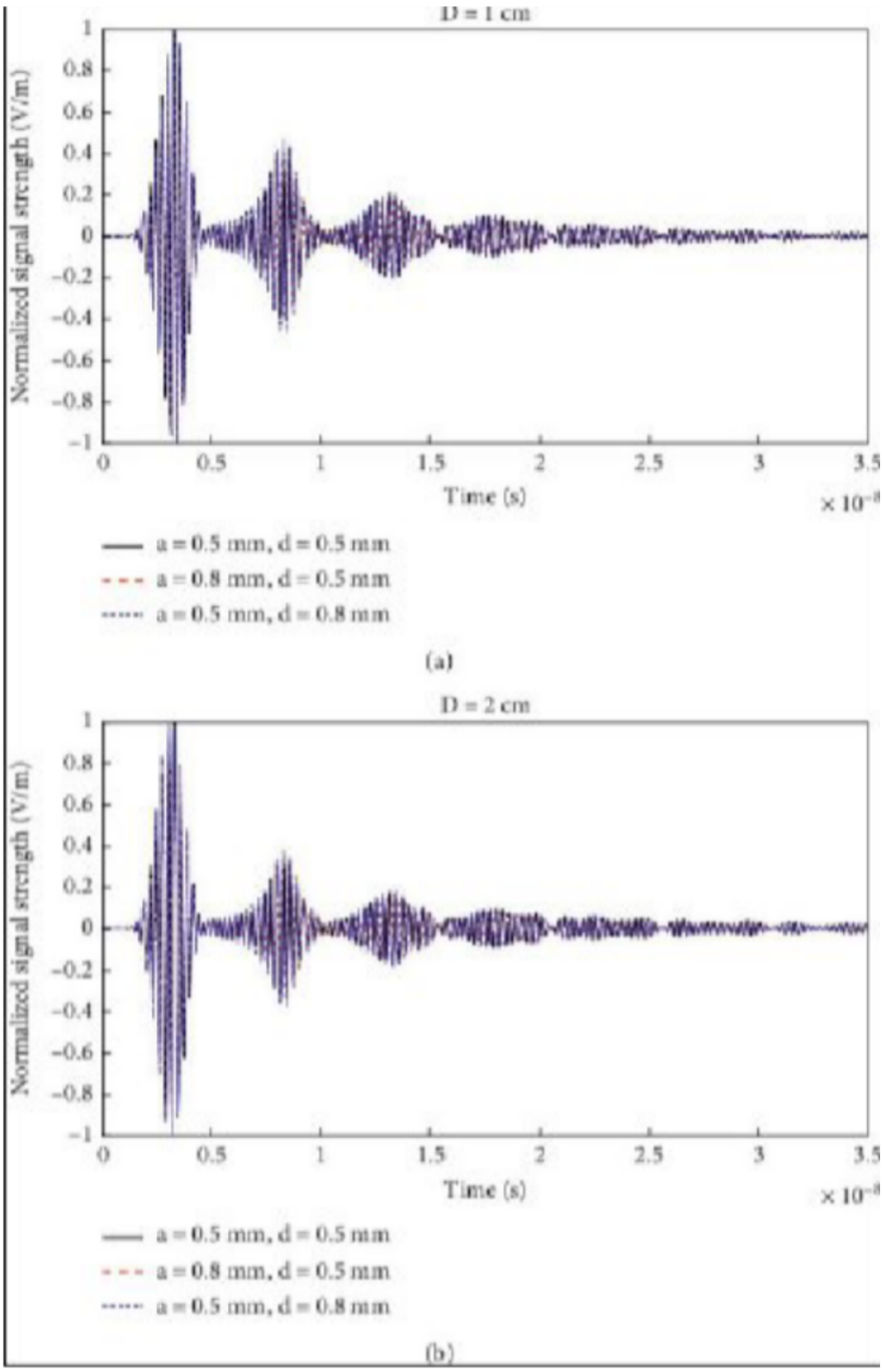

Figure 3.12: Reflected signals for different corrugation profiles at $D = 1$ cm and $D = 2$ cm.

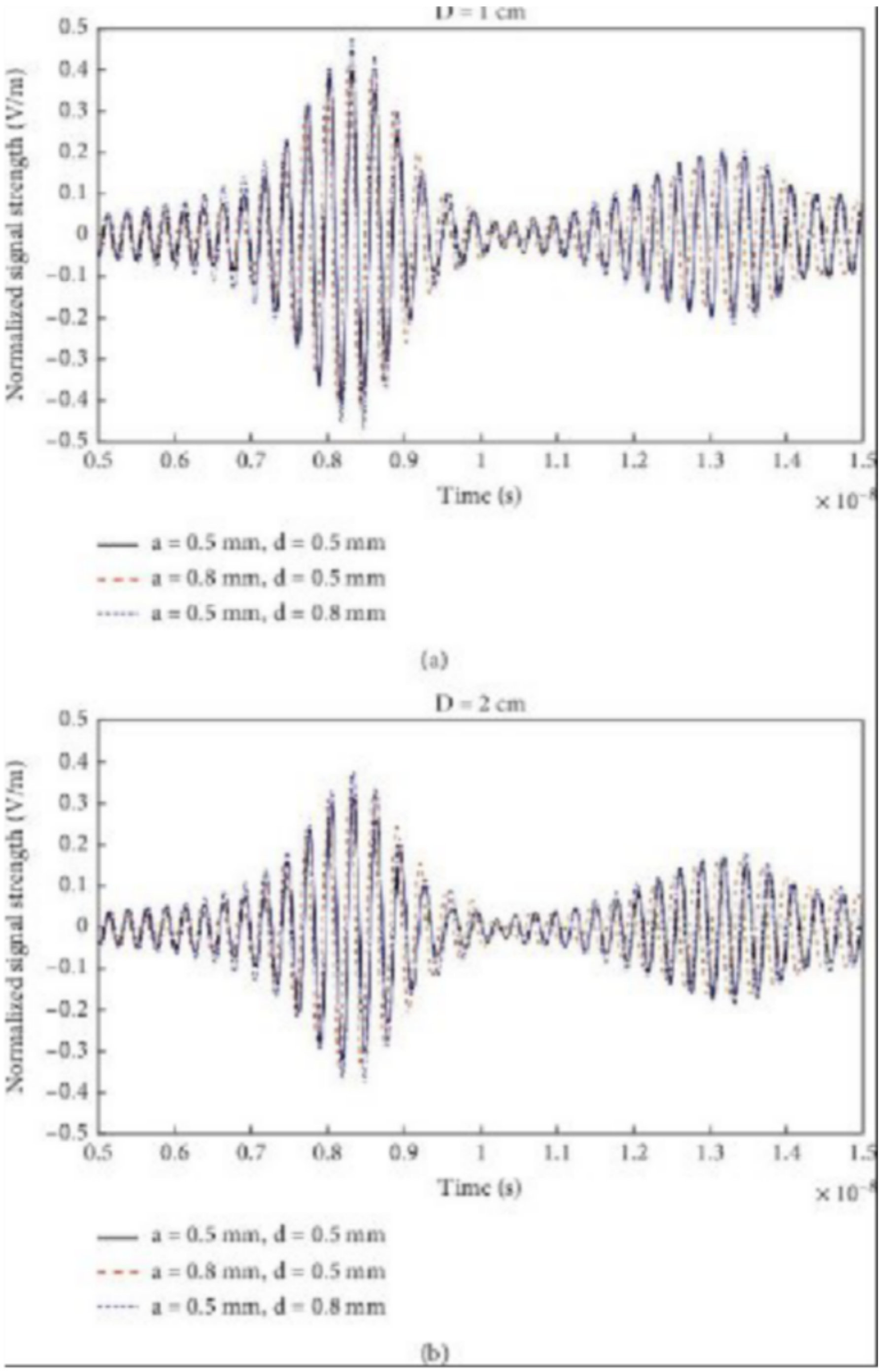

Figure 3.13: Zoomed comparison showing that $a = 0.5$ mm and $d = 0.5$ mm provide the lowest reverberation.

3.6 Comparative Synthesis

Table 3.1: Comparative synthesis of the antenna-to-head distance results.

Distance	Impedance and matching	Field penetration	SAR safety	Reflected signal quality
1 cm	Strongest head loading and most disturbed input impedance.	Strong superficial field but faster decay with depth.	Most restrictive case; permissible input power about 0.13 W.	Strong reverberation and higher clutter level.
2 cm	Moderate loading and more stable impedance behaviour.	Best compromise between penetration and reduced superficial reflection.	Safer condition; permissible input power about 0.28 W.	Cleaner waveform and reduced reverberation.
4.5 cm	Response close to free-space behaviour.	Lower field reaching the head because of distance.	Lower SAR concern.	Weaker useful signal due to spreading loss.

The recommended distance is

$$D_{\text{opt}} = 2 \text{ cm}. \tag{3.11}$$

When combined with Eq. (3.10), this distance gives the best compromise among the tested configurations.

3.7 Scientific Discussion

The results demonstrate that antenna positioning is a primary design parameter in microwave brain imaging. Placing the antenna at 1 cm increases coupling but also increases loading, SAR, and clutter. Placing it at 4.5 cm reduces loading but weakens the useful scattered signal. The intermediate distance 2 cm offers the best balance between coupling, penetration, safety, and signal clarity.

The corrugation study also shows that frequency-domain matching alone is not sufficient. In time-domain imaging, reverberation and pulse fidelity are essential because the diagnostic information is contained in the backscattered waveform. The optimized corrugation profile reduces ringing and improves the quality of the received signal.

3.8 Conclusion

This chapter presented the final simulation results of the proposed antipodal Vivaldi antenna in a microwave brain imaging scenario. The antenna-to-head distance was shown to strongly affect electromagnetic coupling, impedance stability, SAR, field penetration, and reflected-signal quality. The results indicate that $D = 2$ cm provides the best compromise, while the corrugation parameters $a = 0.5$ mm and $d = 0.5$ mm reduce reverberation. Therefore, the recommended configuration is a 2 cm antenna-to-head distance combined with the optimized corrugation profile.

General Conclusion

This thesis investigated the impact of antenna position on the performance of microwave brain imaging for medical diagnosis. The work focused on a compact antipodal Vivaldi antenna because this antenna family provides wide bandwidth, directional radiation, compact geometry, and good suitability for near-field biomedical imaging.

The first chapter presented the physical basis of microwave brain imaging, including propagation in biological tissues, dielectric contrast, scattering, and safety constraints. The second chapter introduced the Vivaldi antenna and explained its geometry, operating principle, substrate selection, and reflection-coefficient behaviour. The third chapter presented the final simulation results and analysed the effect of antenna-to-head distance and corrugation geometry.

The main conclusion is that antenna position strongly influences both electromagnetic performance and biomedical safety. At $D = 1$ cm, the antenna is strongly coupled to the head but suffers from stronger loading, reverberation, and SAR constraints. At $D = 4.5$ cm, the antenna is less perturbed but the useful signal is weaker. The intermediate distance $D = 2$ cm provides the best compromise between coupling, penetration, safety, and reflected-signal clarity.

The corrugation optimization confirmed that the parameters $a = 0.5$ mm and $d = 0.5$ mm reduce reverberation while preserving wideband behaviour. Future work should include experimental validation with a physical head phantom, realistic heterogeneous head models, multi-antenna array analysis, and advanced image-reconstruction algorithms for anomaly localization.

Bibliography

[1] C. A. Balanis, *Antenna Theory: Analysis and Design*, 4th ed. Hoboken, NJ: Wiley, 2016.

[2] D. M. Pozar, *Microwave Engineering*, 4th ed. Hoboken, NJ: Wiley, 2011.

[3] C. A. Balanis, *Advanced Engineering Electromagnetics*, 2nd ed. Hoboken, NJ: Wiley, 2012.

[4] H. G. Schantz, *The Art and Science of Ultra-Wideband Antennas*. Norwood, MA: Artech House, 2005.

[5] S. Gabriel, R. W. Lau, and C. Gabriel, "The dielectric properties of biological tissues: II. Measurements in the frequency range 10 Hz to 20 GHz," *Physics in Medicine and Biology*, vol. 41, no. 11, pp. 2251–2269, 1996.

[6] S. Y. Semenov, "Microwave tomography: review of the progress towards clinical applications," *Philosophical Transactions of the Royal Society A*, vol. 367, pp. 3021–3042, 2009.

[7] E. C. Fear, X. Li, S. C. Hagness, and M. A. Stuchly, "Confocal microwave imaging for breast cancer detection: localization of tumors in three dimensions," *IEEE Transactions on Biomedical Engineering*, vol. 49, no. 8, pp. 812–822, 2002.

[8] K. R. Foster and H. P. Schwan, "Dielectric properties of tissues and biological materials: a critical review," *Critical Reviews in Biomedical Engineering*, vol. 17, no. 1, pp. 25–104, 1989.

Abstract

Medical microwave brain imaging is an emerging non-ionizing technique for detecting neurological abnormalities such as stroke, haemorrhage, and brain tumours. This thesis studies the influence of antenna position on the performance of a compact antipodal Vivaldi antenna used for microwave brain imaging. Different antenna-to-head distances are analysed using full-wave electromagnetic simulation. The results show that $D = 1$ cm provides strong coupling but causes higher reverberation and stricter SAR constraints, while $D = 4.5$ cm weakens the useful received signal. The intermediate distance $D = 2$ cm provides the best compromise between signal quality and safety. The study also shows that optimized side corrugations with $a = 0.5$ mm and $d = 0.5$ mm reduce reverberation while maintaining wideband behaviour.

Keywords: microwave brain imaging; Vivaldi antenna; ultra-wideband antenna; antenna positioning; SAR; reflected signal; biomedical imaging.

Résumé

L'imagerie cérébrale par micro-ondes est une technique non ionisante prometteuse pour la détection d'anomalies neurologiques telles que les AVC, les hémorragies et les tumeurs cérébrales. Ce mémoire étudie l'influence de la position de l'antenne sur les performances d'une antenne Vivaldi antipodale compacte destinée à l'imagerie cérébrale par micro-ondes. Les résultats montrent que la distance $D = 1$ cm fournit un couplage fort mais augmente la réverbération et les contraintes de SAR, tandis que $D = 4.5$ cm affaiblit le signal utile reçu. La distance intermédiaire $D = 2$ cm représente le meilleur compromis entre qualité du signal et sécurité. L'optimisation des corrugations latérales avec $a = 0.5$ mm et $d = 0.5$ mm réduit également la réverbération tout en conservant le comportement large bande de l'antenne.

Mots-clés : imagerie cérébrale par micro-ondes; antenne Vivaldi; antenne ultra large bande; positionnement d'antenne; SAR; signal réfléchi.